Available online at www.sciencedirect.com

ScienceDirect

Procedia Structural Integrity 28 (2020) 1321–1328

Structural Integrity Procedia

www.elsevier.com/locate/procedia

1st Virtual European Conference on Fracture

# In-situ measurements of fatigue damage evolution by electrical resistance method

Riccardo Nobile[a], Andrea Saponaro[a]*

[a]*Department of Engineering for Innovation, University of Salento, Via per Monteroni, 73100 Lecce, Italy*

**Abstract**

Fatigue damage is one of the main failure mechanisms of structures. In the present work Electrical Resistance Changes (ERC) were measured during fatigue tests on notched carbon steel specimens. ERC measurements were performed by monitoring the change in electrical resistance in real-time without interrupting the test at various pre-selected time intervals. The temperature of the specimens was also on-line monitored during the test in order to deduce its effect on the electrical resistance. The comparison of the resistance data measured at initial and different phases of fatigue tests showed the existence of temporal variations associated to fatigue damage: in particular the resistance first decreases, in the initial stages of loading, and subsequently, starting approximately from half-life presents an increase with the number of load cycles due to the internal micro-damage's accumulation. In the final stages of the fatigue test, prior the final fracture, it increases rapidly, in the propagation phase of the crack. In conclusion, the applied experimental method proved to be valid for studying the evolution of damage and to predict and evaluate fatigue life effectively.



*Keywords:* Fatigue of metals; NDE; Damage evolution; Electrical properties.

## 1. Introduction

The mechanical components are subjected to time-varying loads and the evaluation of their structural integrity for the entire useful life is an important challenge to be achieved. With this in mind, there are several techniques for

* Corresponding author. Tel.: +39 0832 297786; fax: +39 0832 297768.
*E-mail address:* andrea.saponaro@unisalento.it


10.1016/j.prostr.2020.10.103

studying the variation of physical material properties induced by fatigue damage within the components in a Structural Health Monitoring (SHM) logic. In literature, various methods have been proposed by researchers to study these phenomena: for example, the change in the electrical resistance of a material subjected to fatigue load has been proposed (Xia et al., (2003)) to evaluate fatigue damage; alternatively, the change in the propagation speed of ultrasound (Omari et al., (2013); Dattoma et al., (2019)) was also used to determine fatigue damage.

The electrical resistance measurement has recently become an active non-destructive evaluation method for damage detection in composites (Park et al., (2001); Park et. al., (2006)). The theory underlying the Electrical Resistance Change (ERC) method is based on Kirchhoff's Law (Xia et al., (2003)). This method not requires expensive equipment for instrumentation and not cause any deterioration of the structure under investigation.

In this work ERC measurements were performed on carbon steel specimens by monitoring the change in electrical resistance in real-time without interrupting the test at various pre-selected time intervals. The comparison of the resistance data recorded at initial and different phases of fatigue tests against the number of load cycles was carried out and associated to the damage accumulation. This repeatable pattern was observed for all specimens tested. The temperature of the specimens was also monitored during the test in order to subtract its effect on the electrical resistance of the specimens. The applied experimental technique proved to be valid for studying the evolution of damage and to predict and evaluate fatigue life of metals effectively.

**Nomenclature**

| | |
|---|---|
| $\sigma_{max.}$ | maximum stress |
| $\Delta R/R_0$ | normalized electrical resistance |
| ERC | Electrical Resistance Change |
| R | load ratio |
| $\alpha$ | temperature coefficient |
| A | resistance temperature coefficient |
| $R_{exp.}$ | experimental resistance |

## 2. Materials and experimental methods

The specimen used in this work for the monitoring of fatigue damage with ERC technique presents a notch in the middle of the gage length and is made in C45 steel (Fig. 1a). Prior to fatigue, a preliminary static test was carried out on a smooth specimen, in displacement control with a velocity of 1 mm/min, in accordance with ASTM E8-04 standard (Fig. 1b). Mechanical properties are summarized in Table 1.

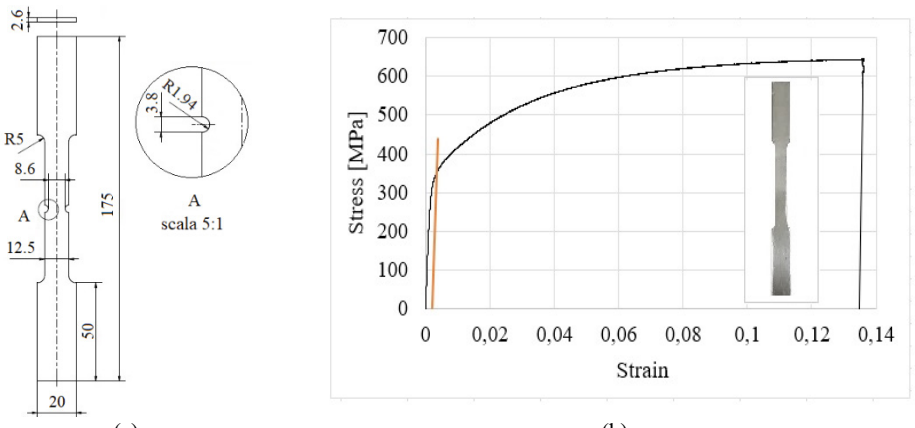


Fig. 1. (a) Notched specimen's geometry for ERC method; (b) Stress-strain curve of the un-notched specimens.

Table 1. Experimentally determined mechanical properties.

| Mechanical Properties | | |
|---|---|---|
| Ultimate Tensile Strength (UTS) | 640 | [MPa] |
| 02% Yield Strength | 350 | [MPa] |
| Young's Modulus | 219953 | [MPa] |
| Poisson's Ratio | 0.29 | |

The experimental set-up for in-situ real time measurements during the fatigue tests includes a DC power supply and a digital data acquisition unit (Fig.2b). In addition, a thermocouple (type T) was applied in the notched section of each specimen in order to measure the temperature during the fatigue tests. In order to measure the resistance, a known direct-current is injected through two electrical contacts in the specimen and the voltage between two electrodes is measured. If a current is injected using the two electrodes, it will choose the path of the least resistance, meaning through the testing machine. In order to prevent this, the test specimen needs to be insulated from the machine. For this purpose, wooden insulating tabs were glued to the end of the specimen, around the gripping area (Fig. 2a). The internal electrodes for measuring the voltage have been fixed to the specimens tested with special tools and screws in steel for optimum electrical contact. Using Ohm's law, it is possible to calculate the electrical resistance on the basis of the value of the voltage decay.

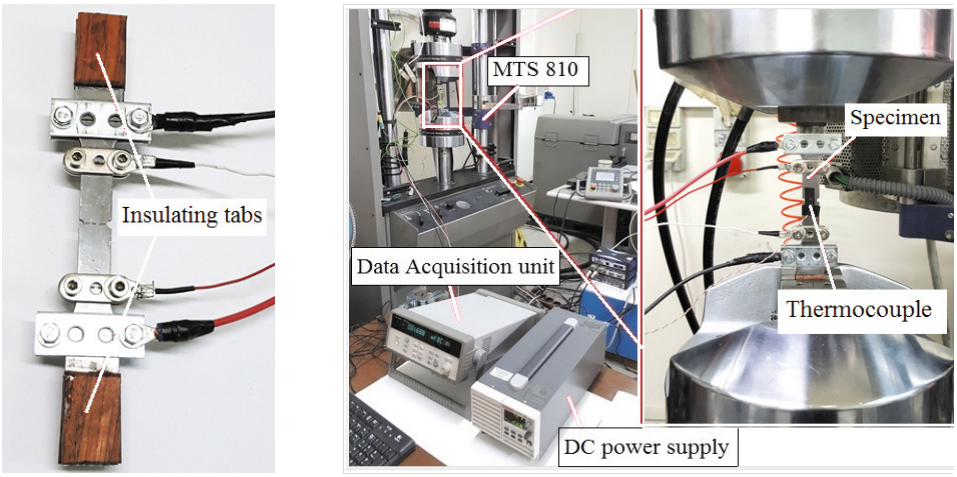


(a) (b)

Fig. 2. (a) Specimen with wooden insulating tabs and electrical contacts; (b) experimental set-up of fatigue test.

Figure 3 shows the 4-wire measuring circuit used in this work. The internal voltage measuring electrodes were positioned at a distance of 25 mm from the center of the notch, while the external current electrodes were located at a distance of 43 mm from it.

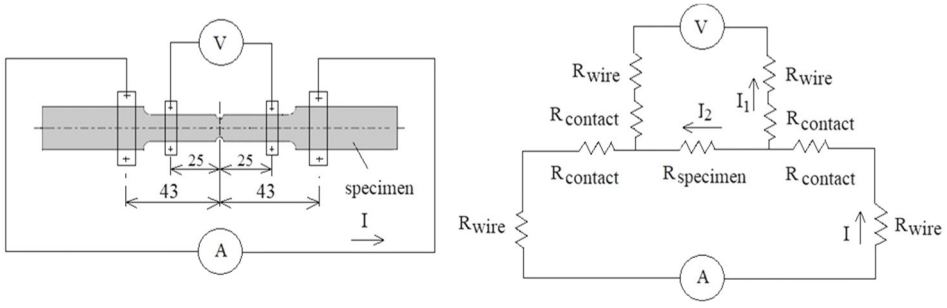


Fig. 3. 4-wire connection technique adopted to measure electrical resistance (dimension in mm).

Four-wire technique was selected in this work to eliminate the parasitic resistance of the cables. The technique uses an outer pair of electrodes to apply electric current and uses an inner pair of electrodes to measure resistance from the voltage drop between them. This setup is also used in (Kupke et al., (2001); Todoroki et al., (2004); Wang et al., (1997)). This method is said to be more accurate than the two-probe technique (Todoroki et al., (2004); De Baere et al., (2010)), but the experimental set-up is more complicated. The type of measurement covered the entire volume of the sample and therefore also the area where the notch is present.

Force-controlled fatigue tests are performed using a MTS 810 servo-hydraulic axial testing machine equipped with a load capacity of ±100 kN in Experimental Mechanic Laboratory at University of Salento (Lecce, Italy) (Fig. 2b). All parameters (voltage, temperature, time, load and displacement) were recorded during the whole test.

The specimens are subjected to sinusoidal tension-tension load cycles with load ratio R = 0.1. The tests were performed under three different load amplitudes, corresponding to different fatigue life. In particular the fatigue parameters were $\sigma_{max}$ = 335.4 MPa and load frequency 10 Hz for specimen $P_1$, $\sigma_{max}$ = 357.78 MPa and load frequency 10 Hz for specimen $P_2$ and $\sigma_{max}$ = 366.73 MPa and load frequency 2 Hz for specimen $P_3$. The first resistance measurement was performed on the unloaded specimen prior the fatigue test and was taken as a reference electric resistance ($R_0$) in order to monitor the progress of the damage. The subsequent measurements were carried out on the specimen in real time with adequate sampling intervals, depending on the expected fatigue life.

## 3. Results and discussion

The effect of the temperature on the electro-mechanical response (electrical resistance change) was also considered to avoid the introduction of unacceptable experimental errors. The real-time recording of the specimen temperature during the fatigue test for the $P_2$ specimen (Fig. 4a) revealed a moderate increase during the fatigue test followed by a rapid increase response in the final fracture stages for the specimens. Since the electrical resistance is temperature dependent, it is evident that temperature effect must be considered to obtain acceptable and comparable resistance measurements during the whole fatigue test. This behavior depends on the material and can be assessed with the α temperature coefficient and the influence of the ΔT temperature increase, as described by Eq. (1):

$$R = R_0(1 + \alpha\Delta T) \tag{1}$$

$R_0$ is the initial resistance, α is the temperature coefficient and $\Delta T = (T\text{-}T_0)$ the temperature difference from the starting point. Manipulating Eq. (1), the expected electrical resistance change due to the temperature can be calculated using Eq. 2 (Vavouliotis et al., (2011)):

$$\Delta R_{Thermal} = A\ x\ \Delta T \tag{2}$$

where $A = R_0\ \alpha = 0.004143$ mΩ $°C^{-1}$ is the resistance temperature coefficient. The resistance temperature coefficient A was experimental measured by heating the specimen from the room temperature of 20 °C to 28 °C (ΔT = 8 °C) and measuring the increase in resistance from $R_0$ = 1.056 mΩ at R = 1.091 mΩ respectively for the carbon steel specimens tested. For each specimen, the voltage recorded experimentally and therefore the resistance ($R_{exp.}$) is the result of the variation of the initial resistance ($R_0$) due to the temperature and that due to the development of the damage:

$$R_{exp} - R_0 = \Delta R_{Thermal} + \Delta R_{Damage} \tag{3}$$

The computed electrical resistance data due to the thermal contribution ($\Delta R_{Thermal}$) has been subtracted from the recorded value of the experimentally resistance ($\Delta R_{exp}$) in order to obtain the resistance value associated to damage:

$$\left(\Delta R_{exp} - \Delta R_{Thermal}\right) = R_0 + \Delta R_{Damage} = R_{Damage} \tag{4}$$

Figure 4a shows the electro-mechanical response $(R/R_0)_{exp.}$, the trend of the correct resistance $(R/R_0)_{Damage}$ due to damage and the resistance due to the increase in temperature $(R/R_0)_{Thermal}$ for $P_2$ specimen. The data were normalized by the reference electric resistance ($R_0$) to avoid the effect of the electrical resistance difference between specimens;

in the same manner, the number of fatigue cycles was normalized respect to the fatigue life of the specimen (number of fatigue cycles/total fatigue life). In particular, 0% of the fatigue life is therefore referred to the specimen before fatigue test while 100% is related to the final fracture of the specimen. For the $P_1$ specimen, the reference resistance $R_0$ was 0.836 mΩ; while for the $P_2$ and $P_3$, specimen the reference resistance $R_0$ was 0.850 mΩ and 0.864 mΩ respectively. Moreover, the time-stability of this set-up was first tested by measuring the resistance of an unloaded specimen for an extended period of time, corresponding with a standard fatigue test. A 2000mA current was injected through the sample $P_1$ and resistance was measured over an extended period of time. The result is represented in Figure 4b. As can be seen, there is no significant increase in endurance over time. During the experiments the temperature was also monitored and there was no significant increase or decrease in the latter (measured temperature increase or decrease was less than 2 °C.). The signal of resistance is fairly stable and the ambient temperature did not affect the measurement system, demonstrating the validity of the 4-wire method.

As can be seen from the graph in Figure 4a, the contribution of temperature for $P_2$ specimen on the electrical resistance is almost negligible. The same behavior was observed for all specimens tested. In particular from the graph (Fig. 4a), a resistance drop was observed during the initial loading stages (30% of fatigue life). Subsequently, an increase in resistance was observed starting from 40% of the life probably due to a deterioration of the material and the formation of micro-crack followed by a rapid increase in the latter to approximately 80% of fatigue life in the propagation phase of the crack until the final specimen fracture at 93492 cycles.

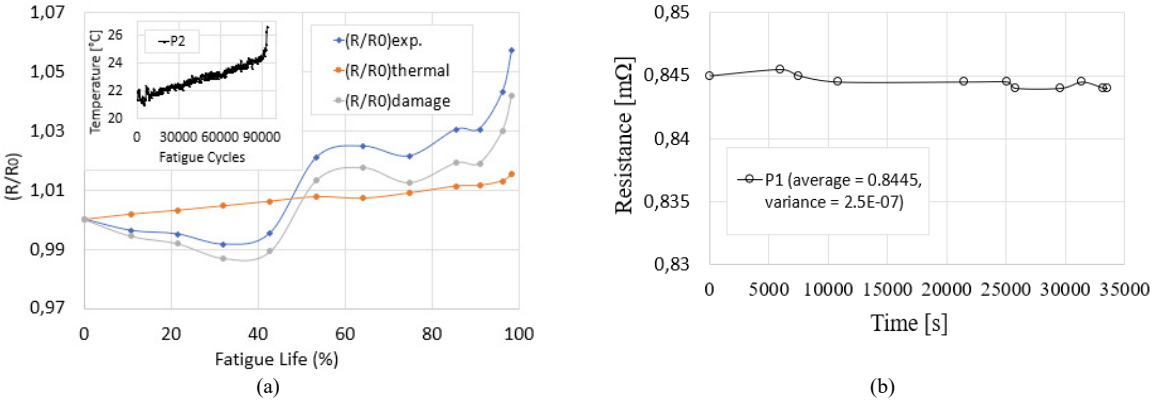


Fig. 4. (a) Normalized resistance (experimental, thermal and damage) against fatigue life (%) and temperature profile during fatigue is also shown in inserted graph for $P_2$ specimen; (b) Resistance trend over time of the unloaded $P_1$ specimen (4-wire method – 2000 mA).

The electrical resistance data recorded were averaged over a period of 1s. As it has been reported in other researches (Vavouliotis et al., (2011); Mi et al., (2006), Kostopoulos et al., (2009)), the resistance monitoring system follows directly with a certain approximation the sinusoidal waveform of the load, as shown in Figure 5 for the specimen $P_3$. The sampling rate of the electrical resistance data was roughly the same of the fatigue data recorded for the $P_3$ sample as can be seen in Figure 5.

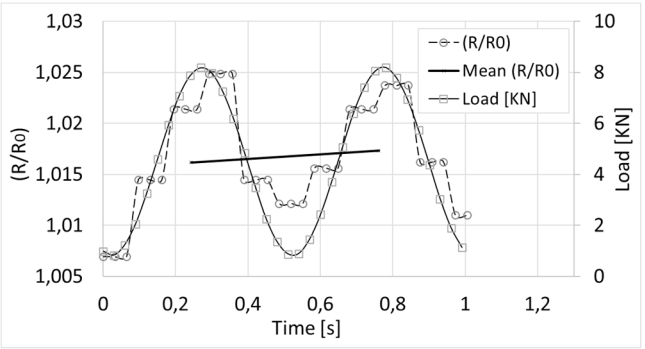


Fig. 5. Graph of the normalized resistance and of the applied load versus time for $P_3$ specimen.

Figure 6 shows the total experimental resistance variation ($R_{exp.}$) which includes both thermal term and that due to damage as the percentage of fatigue life changes. Figure 7a shows for all specimens the experimentally obtained results of normalized electrical resistance change due to only damage, expressed as a change in resistance divided by the reference resistance ($(R-R_0)/R_0$), versus fatigue life percent.

Generally, all curves show a similar trend. For $P_1$ specimen, the total resistance decreases starting from 0% up to 30% of the fatigue life, presenting an increase from 40%, probably due to internal micro-damages accumulation.

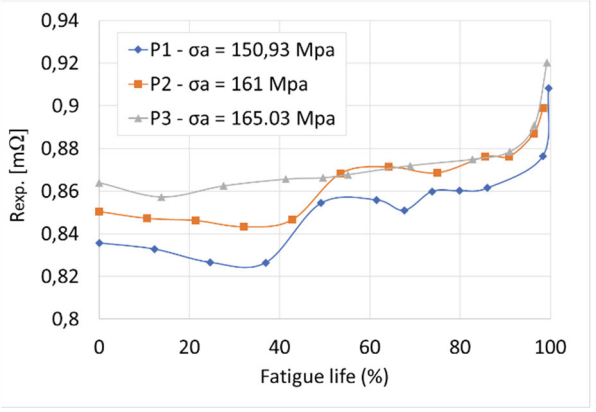


Fig. 6. Experimental resistance changes for $P_1$, $P_2$ and $P_3$ specimens against fatigue life (%).

Subsequently, starting from 85% of fatigue life, the resistance increases rapidly until the sample fracture, during the crack propagation phase. For the $P_2$ specimen, the total resistance decreases from the start of the test up to 30%. From 43% it starts to increase. Subsequently, the electrical resistance increases rapidly in the final stages before failure to 80-90%, in the damage propagation phase. The specimen $P_3$ also showed a similar behaviour to the previous ones but the resistance curve on the whole appears flatter, with less marked variations compared to the first two samples tested ($P_1$ and $P_2$). In particular, the resistance decreases starting from 0% to 15%. It gradually increases from 30% of fatigue life and then presents a rapid increase of the same from 82% until the final failure.

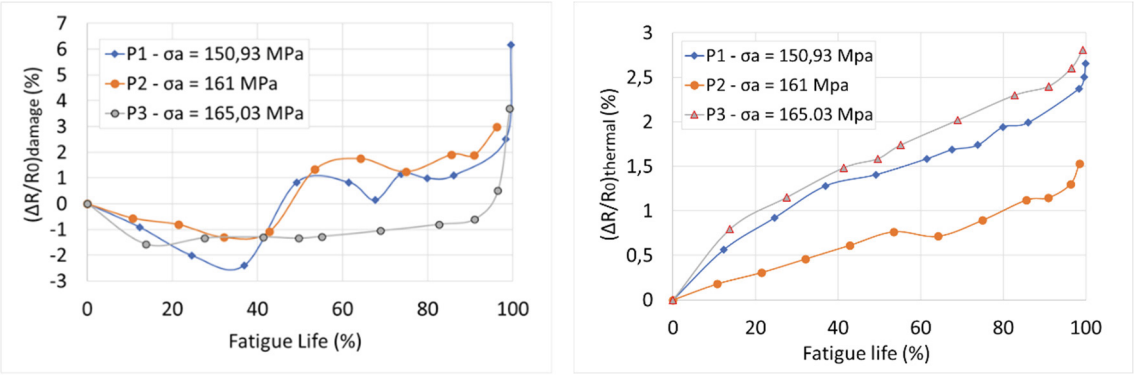


(a) (b)

Fig. 7. (a) Normalized electrical resistance trends due to only damage and (b) normalized resistance due to the thermal effect versus fatigue life for various specimens at different load levels.

A repeated behaviour pattern was confirmed during fatigue tests: during the initial loading phases, the resistance drops and subsequently increases, first gradually and then abruptly until the final failure, in the crack propagation phase. This resistance variation was recorded until the final failure for all specimens. The thermal contribution to the electrical resistance changes was greater on the specimen $P_3$ since the latter was subjected to a higher level of stress.

From the graph of Fig. 7a, the increase of resistance due to damage starting from about half-fatigue life was observed for the specimen $P_3$, although to a less obvious extent than the other two samples tested. Fig. 7b instead shows the

trends of ERC due to temperature term as the percentage of fatigue life vary. From the graph it is clear that the specimen $P_3$ has the greatest resistance variation due to the thermal contribution compared to the other two samples.

By processing fatigue data, the stiffness for all specimens was determined as load cycle varied. Figure 8 shows the trend of normalized stiffness with respect to its initial value as a function of the percentage of fatigue life. The curves referred to specimens $P_1$ e $P_2$ present an almost constant first part and a reduction from approximately 85% of fatigue life. Subsequently, starting from 95% of fatigue life, stiffness decreases rapidly until the specimen's failure. For $P_1$ specimen the final failure was reached at 162686 cycles while for the $P_2$ specimen at 93492 cycles.

The stiffness reduction for $P_3$ specimen was observed starting from 25000 cycles (70% of fatigue life), first gradually up to 90% of fatigue life and then rapidly, until the final specimen fracture occurred at 36281 cycles.

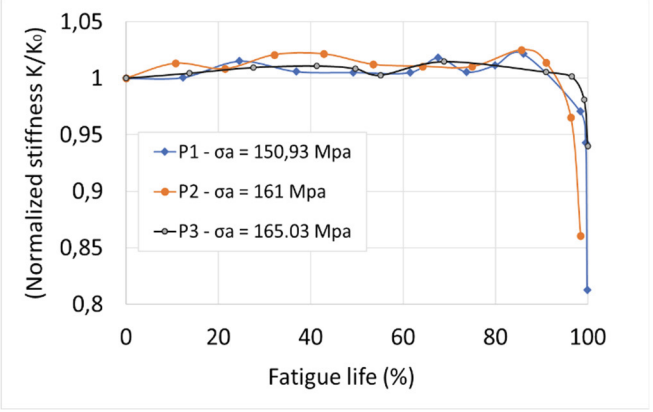


Fig. 8. (a) Normalized stiffness ($K/K_0$) versus fatigue life (%).

The on-line recording of the specimen's temperature during the fatigue loading summarized in Figure 9 for all specimens revealed a constant increase at the initial stages of loading followed by an increase trend till the final failure. In particular, for the specimen $P_1$, the acquired temperature data showed a 5 °C increase for 95% of the fatigue life, presenting a rapid increase up to 7 °C before the final failure. Specimen $P_2$ shows a lower temperature variation. It increases by about 3 °C for 93% and under-goes a rapid increase up to 5 °C before the final failure. $P_3$ specimen exhibits greater temperature variations. The temperature recordings showed a faster increase for 90% of 5.7 °C, rapidly increasing up to about 7 °C in the final stages before the fracture.

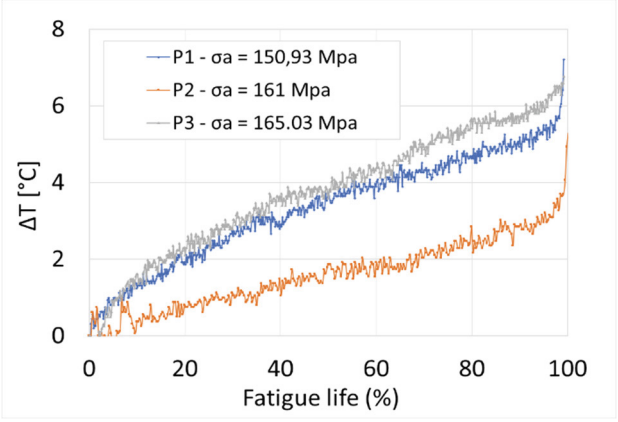


Fig. 9. Temperature variation versus fatigue life (%) for all specimens tested.

Figure 10 show an example of fracture surface with visible cracks highlighted on the side A (Fig. 10a) and the side B (Fig. 10b), observed with the stereo microscope after fatigue for the $P_1$ specimen.

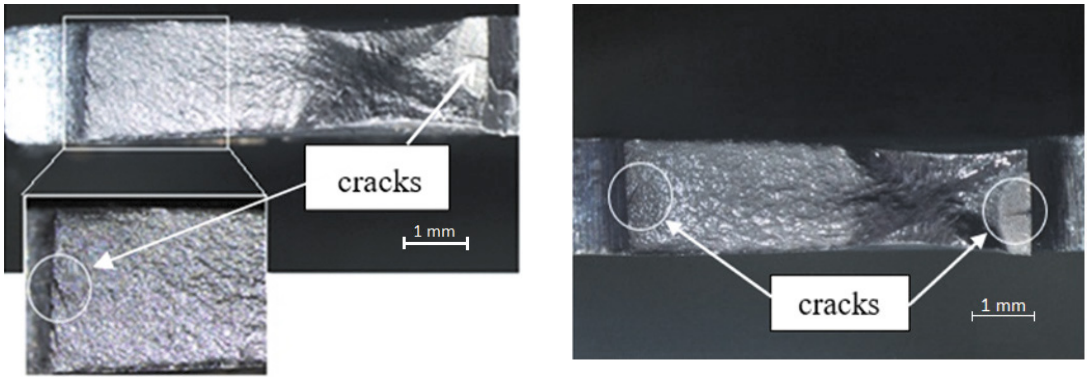


(a) (b)

Fig. 10. Fracture surface analysis by stereo microscope. (a) Side A and (b) Side B after fatigue test for the $P_1$ specimen.

## 4. Conclusions

In the present work, the electrical resistance technique was used for real-time monitoring of damage in carbon-steel specimens subjected to dynamic cyclic loads.

Increases of electrical resistance were monitored and recorded in different stages during the fatigue life. From the electrical resistance measurements carried out on the batch of tested specimens, it is shown that the resistance first decreases in the initial stages of loading and subsequently, starting approximately from half-life, presents an increase, probably due to the internal micro-damage's accumulation. In the final stages of the fatigue test, prior the final fracture, it increases rapidly, in the propagation phase of the crack. This behavior was observed for all tested samples. Moreover, the tests have shown that the effects of the temperature and the injected current on the resistance increase, due to only damage, are negligible for the different load conditions adopted.

Results shown that the electrical resistance method is valid to monitor and predict with accuracy the fatigue damage progress of metals.

## References

Dattoma, V., Nobile, R., Panella, F.W., Saponaro, A., 2019. Real-time monitoring of damage evolution by nonlinear ultrasonic technique, Procedia Structural Integrity 24, 583-592.

De Baere, I., Van Paepegem, W., Degrieck, J., 2010. Electrical resistance measurement for in situ monitoring of carbon fabric composites. International Journal of Fatigue 32, 97-207.

Kostopoulos, V., Vavouliotis, A., Karapappas, P., Tsotra, P., Paipetis, A., 2009. Damage monitoring of carbon fiber reinforced laminates using resistance measurements. Improving sensitivity using carbon nanotube doped epoxy matrix system. J Intell Mater Syst Struct 20(9), 1025-1034.

Kupke, M., Schulte, K., Schuler, R., 2001. Non-destructive testing of FRP by d.c. and a.c. electrical methods. COMPOSITES SCIENCE AND TECHNOLOGY 61 (6), 837-847.

Mi, B., Michaels, J.E., Michaels, T.E., 2006. An ultrasonic method for dynamic monitoring of fatigue crack initiation and growth, The Journal of the Acoustical Society of America, 119 (1), 74-85.

Omari, M. A., Sevostianov, I., 2013. Estimation of changes in the mechanical properties of stain-less steel subjected to fatigue loading via electrical resistance monitoring. International Journal of Engineering Science 65, 40-45.

Park, J.-M., Lee, S.-I., DeVries, K.L., 2006. Nondestructive sensing evaluation of surface modified single-carbon fiber reinforced epoxy composites by electrical resistivity measurement. Compos Part B Eng. 37, 612-626.

Park, J.-M., Lee S.-I., Kim K.W., Yoon D.J., 2001. Interfacial aspects of electrodeposited conductive fibers/Epoxy composites using electro-micromechanical technique and nondestructive evaluation. J Colloid Interface Sci. 237 (1), 80-90.

Todoroki, A., Yoshida, J., 2004. Electrical resistance change of unidirectional CFRP due to applied load. JSME INTERNATIONAL JOURNAL SERIES A-SOLID MECHANICS AND MATERIALS ENGINEERING 47 (3), 357-364.

Vavouliotis, A., Paipetis, A., Kostopoulos, V., 2011. On the fatigue life prediction of CFRP laminates using the Electrical Resistance Change method. Composites Science and Technology. 71, 630-642.

Wang, X.J., Chung, D.D.L., 1997. Real-time monitoring of fatigue damage and dynamic strain in carbon fiber polymer-matrix composite by electrical resistance measurement, SMART MATERIALS & STRUCTURES 6 (4), 504-508.

Xia, Z., Okabe, T., Park, J.B., Curtin, W.A., Takeda, N., 2003. Quantitative damage detection in CFRP composites: coupled mechanical and electrical models. Compos Sci Technol 63, 1411-1422.